

LARGE-EDDY SIMULATION OF ACCELERATED TURBULENT FLOW IN A PIPE

Seo Yoon Jung

Mechanical Engineering,
Imperial College London
London, SW7 2AZ, U.K.
s.jung@imperial.ac.uk

Yongmann M Chung

School of Engineering and Centre for Scientific Computing,
University of Warwick
Coventry, CV4 7AL, U.K.
Y.M.Chung@warwick.ac.uk

ABSTRACT

Large-eddy simulations of unsteady turbulent pipe flows were performed to investigate the response of near-wall turbulence to temporal acceleration. The simulations were started with the fully-developed turbulent pipe flow, and then a constant temporal acceleration was applied. The Reynolds number of the pipe flow, based on the pipe diameter and the bulk-mean velocity, increased linearly from $Re_D = 7000$ to 45200. Various turbulence statistics revealed distinctive features of the delays responsible for turbulence production, energy redistribution, and radial propagation. It was found from the LES results that turbulent viscosity was frozen in the early transient, followed by a rapid increase. This delay was due to the slow response of the wall shear stress and Reynolds shear stress. The vorticity field showed the delayed response of the near wall structures after the onset of temporal acceleration.

INTRODUCTION

Unsteady turbulent flows through a pipe are often encountered in engineering applications such as turbomachinery and heat exchangers, and also in blood flows in large arteries. In addition to the practical implications of achieving a better understanding of flows of this type, the study of unsteady turbulent flows in pipes provides insight into the underlying physics of turbulent boundary layers. To date, unsteady turbulent flows have received relatively little attention compared to steady ones despite their importance. Many experimental and numerical studies of unsteady turbulent pipe flows have focused on periodic pulsating flows rather than non-periodic transient ones.

As regards the non-periodic transient pipe flow, Kataoka *et al.* (1975) have investigated the sudden response to a step input of flow rate using an electrochemical technique. They found that the time at which transition from laminar to turbulent state occurred decreases with increasing Reynolds number. Maruyama *et al.* (1976) carried out an experiment in similar conditions to that of Kataoka *et al.* (1975). They observed the delay in the response of turbulence, which was found to be propagated from the wall to the centre of the pipe. A study of He and Jackson (2000) was concerned with flow transients with increasing and decreasing flow rate in a pipe using LDV. They observed three delays in the turbulence: a delay in the turbulence production, a delay in turbulence energy redistribution, and a delay

related to the radial propagation of turbulence. Moreover, they revealed that the radial propagation of turbulence is determined by initial flow conditions. Greenblatt and Moss (2004) measured the turbulent pipe flow with a temporal pressure gradient change which was larger than those considered in the previous studies.

A perusal of the relevant literature indicates that numerical studies on the transient turbulent flow with temporal pressure gradient are relatively scarce. Recently, a DNS of a decelerated turbulent channel flow subjected to a sudden change of pressure gradient was performed by Chung (2004). He found that there are two different relaxations in the flow: a fast relaxation at the early stage and a slow one at the later stage. Moreover, the anisotropic response of the near-wall turbulence was detected in the early stage, which would be a troublesome problem to standard turbulence models (Chung and Jafarian, 2005). In the present work, a series of large-eddy simulations of an accelerated turbulent pipe flow were performed to elucidate the delay effect on the near-wall turbulence. Various turbulence statistics were analysed to study the response of the near-wall turbulent flow.

NUMERICAL METHODS

The filtered incompressible Navier-Stokes equations are solved:

$$\frac{\partial \bar{u}_i}{\partial x_i} = 0, \quad (1)$$

$$\frac{\partial \bar{u}_i}{\partial t} + \frac{\partial}{\partial x_j} (\bar{u}_i \bar{u}_j) = -\frac{\partial \bar{p}}{\partial x_i} + \frac{1}{Re} \frac{\partial^2 \bar{u}_i}{\partial x_j \partial x_j} + f \delta_{i1}, \quad (2)$$

where the overbar denotes a filtered variable, f is the acceleration parameter, and τ_{ij} is the subgrid-scale stress:

$$\tau_{ij} = \overline{u_i u_j} - \bar{u}_i \bar{u}_j, \quad (3)$$

All the variables are non-dimensionalised by the radius of the pipe (R) and the bulk mean velocity at the initial Reynolds number (U_{m0}). Here, the subscript 0 indicates values at the initial Reynolds number. In Equation (2), the acceleration parameter was set to be $f = 0$ for a steady turbulent flow, and f had a positive value when the flow was accelerated. The numerical method in cylindrical coordinates requires significant effort to treat the singularity at $r = 0$. In the present formulation, the radial flux $q_r = r u_r$ on a staggered grid was introduced to simplify the discretisation of this region, since $q_r = 0$ at $r = 0$ (Vericco and Orlandi, 1996). In

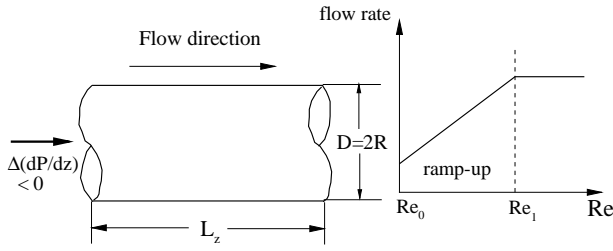


Figure 1: A schematic diagram of computational domain.

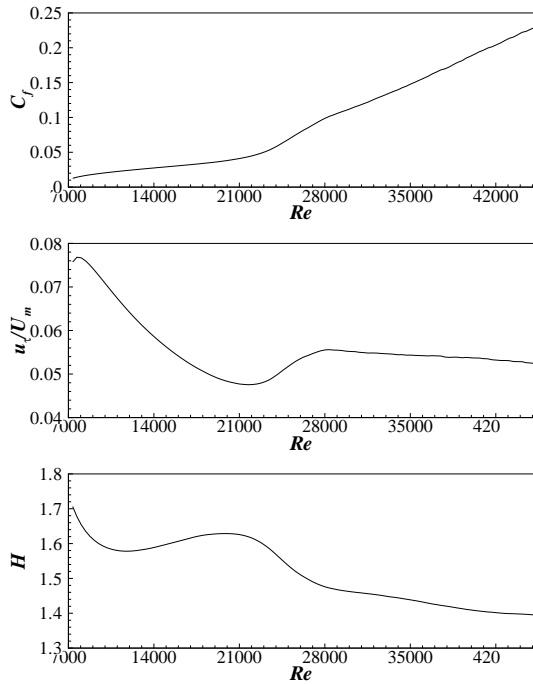


Figure 2: Time histories of skin friction coefficient C_f , u_τ/U_m , and shape factor H .

the present study, the simulations were started from a fully-developed turbulent pipe flow ($f = 0$) at $Re_{D0} = 7000$: here the Reynolds number ($Re_{D0} = U_{m0}D/\nu$) is based on the pipe diameter and the bulk-mean velocity. The acceleration parameter f was kept constant throughout the calculations, so the mass flow rate was increased linearly to the final Reynolds number of $Re_{D1} = 45200$, as shown in Fig. 1. The dimensionless parameter $\gamma = D/u_{\tau 0}(1/U_{m0} \cdot dU_{m0}/dt)$ proposed by He and Jackson (2000), which provides an indication of the departure from the turbulence of pseudo-steady flow, was selected as 6.1. These parameters were chosen to compare the results with the experimental data of He and Jackson (2000), and the corresponding acceleration parameter used in Equation (2) was $f = 0.2$.

The computational domain in the streamwise direction was $L = 8R$. The number of grid points in the x , r , and θ directions was $129 \times 257 \times 257$ respectively. In the wall-normal direction, grid points were clustered according to a hyperbolic tangent distribution. The mesh resolutions were $\Delta x^+ = 14.38$ and 74.38 , $\Delta y_{min}^+ = 0.02$ and 0.10 , $\Delta y_{max}^+ = 2.90$ and 14.90 , and $\Delta z^+ = 5.65$ and 29.20 at the initial ($Re_{D0} = 7000$) and the final Reynolds numbers

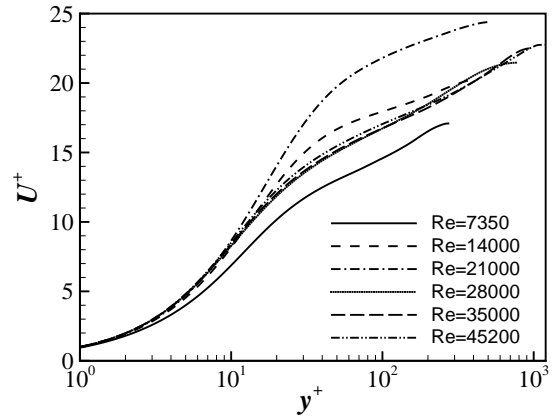
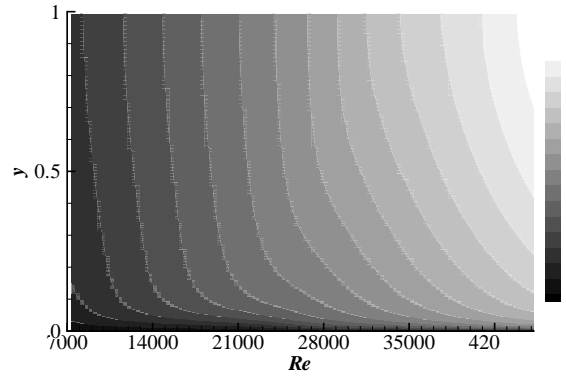


Figure 3: Mean velocity profiles.

($Re_{D1} = 45200$) respectively. Periodic boundary conditions were applied in the axial and circumferential directions for the velocity components, and a no-slip boundary condition was imposed at the solid walls. The time step was $0.0005R/U_{m0}$ and the total excursion time was $27.2R/U_{m0}$. The ensemble averages were based on databases consisting of eight independent realisations.

A dynamic subgrid-scale stress model was used to account for subgrid-scale stresses (Germano *et al.*, 1991; Lilly, 1992). The model constant C was averaged over the x and θ directions. The grid filter width Δ was taken to be equal to the grid spacing. The test filter was a box filter in real space, applied by a three-point averaging using Simpson's rule. The box filter was applied in the streamwise and azimuthal directions. No explicit test filtering was applied in the radial direction. The total viscosity $1/Re + \nu_t$ was constrained to be non-negative to ensure numerical stability of the time integration.

The governing equations were integrated in time using the fractional step method with the implicit velocity decoupling procedure proposed by Kim *et al.* (2002). In this approach, the terms in the momentum equations were first discretised in time using the Crank-Nicolson method, and then the coupled velocity components in the convection terms were decoupled using the implicit velocity decoupling procedure. The decoupled velocity components were then solved without iteration. Because the implicit decoupling procedure relieved the Courant-Friedrichs-Lewy (CFL) restriction, the computation time was reduced significantly. The computational time of the iterative scheme was 1.6-1.9

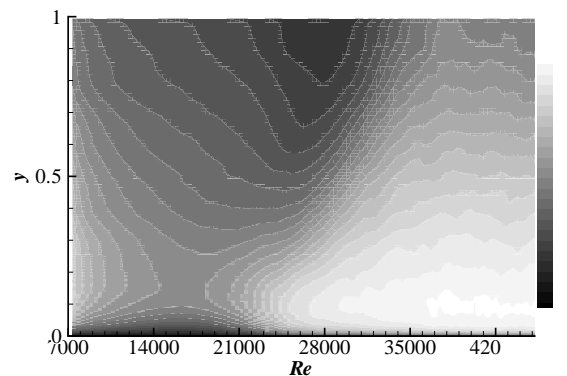
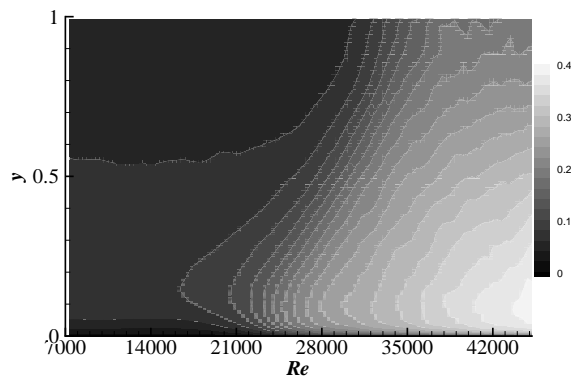
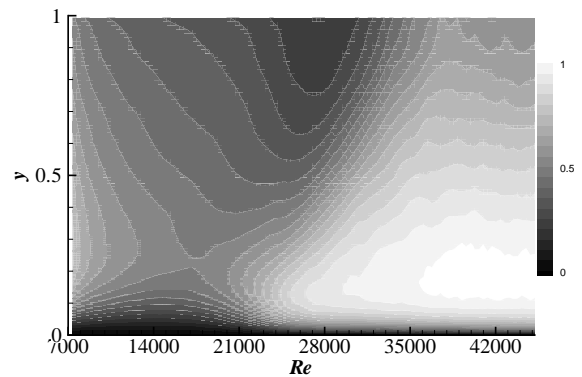
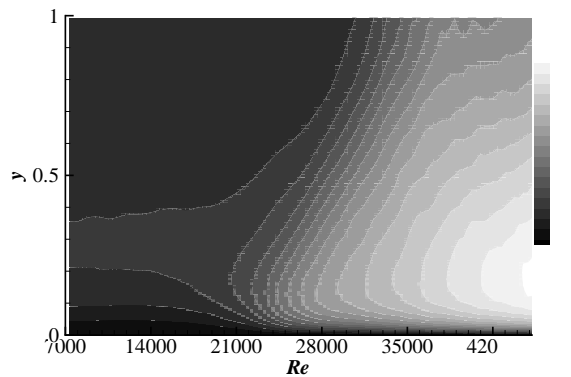
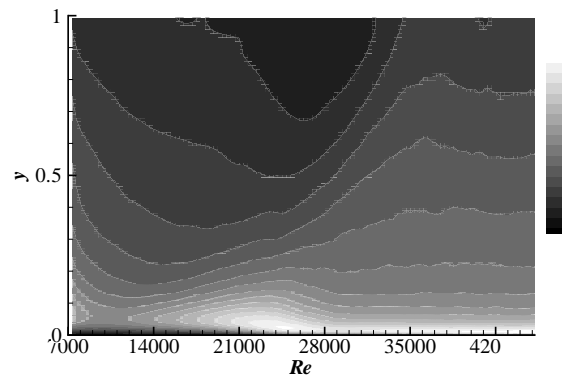
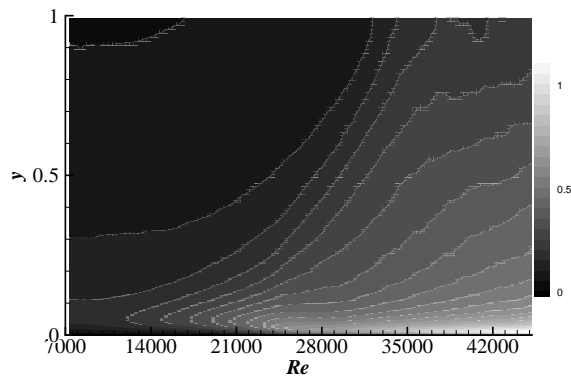


Figure 4: Velocity fluctuations normalised by the initial bulk-mean velocity, u_{rms}/U_{m0} , v_{rms}/U_{m0} and w_{rms}/U_{m0} .

Figure 5: Velocity fluctuations in wall units normalised by the local friction velocity, u_{rms}^+ , v_{rms}^+ and w_{rms}^+ .

times larger than that of Kim *et al.* (2002). The overall accuracy in time was second-order. All the terms were resolved using a second-order central difference scheme in space with a staggered mesh.

RESULTS AND DISCUSSION

First, numerical simulations of turbulent pipe flows at several Re numbers were conducted using DNS and LES to ascertain the reliability and accuracy of the present numerical simulations. The present DNS and LES results are in excellent agreement with the existing DNS data of Akselvoll and Moin (1996) and Wu and Moin (2008). In addition, the unsteady mean velocity profiles at several Re numbers from the unsteady simulations were compared with the experimental data of He and Jackson (2000). The numerical and

experimental results are in good agreement, and the small discrepancy between the simulation and the experiment at high Re might be owing to the experimental uncertainties in mean velocity measurement (10%). The velocity fluctuations were also compared with the experimental data at several radial locations and are in good qualitative agreement with the experiment (Chung and Jung, 2008).

Mean Properties

Figure 2a) shows the development of the skin friction coefficient $C_f = \tau_w / (0.5U_{m0}^2)$. The response of the wall shear stress to the temporal acceleration can be divided into three different stages: an initial weak time-dependence (WT) stage, a strong time-dependence (ST) stage, and a pseudo-steady (PS) stage. Since the mass flow rate increases

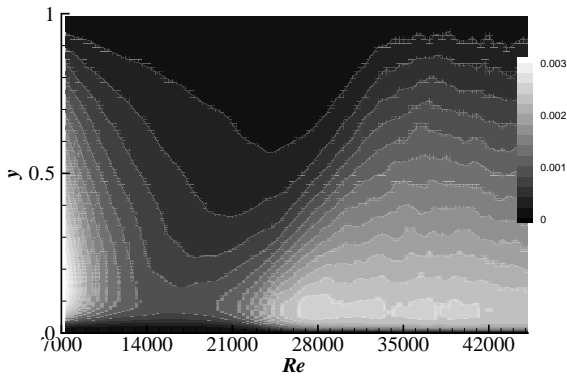


Figure 6: The Reynolds shear stress normalised by the local bulk-mean velocity, $-\overline{uv}/U_m^2$.

linearly in time, the local Reynolds number is equivalent to the time elapsed after onset of the acceleration. The initial weak time-dependence stage ($7000 < Re_D < 21000$, or $0 < tU_{m0}/R < 10$) denotes the gradual increase of C_f due to slower responses of turbulence than those of the mean velocity. During the strong time-dependence stage ($21000 < Re_D < 28000$, or $10 < tU_{m0}/R < 15$), the turbulence production near the wall is vigorously enhanced, thus C_f is rapidly increased. In the pseudo-steady stage ($Re_D > 28000$, or $tU_{m0}/R > 15$), the turbulence approaches the pseudo-steady state near the wall and it is propagated from the wall to the centre of the pipe at a certain speed.

The friction velocity normalised by the local bulk-mean velocity, u_τ/U_m is also shown in Figure 2. The friction velocity is related to the skin-friction coefficient: $\frac{u_\tau}{U_m} = \sqrt{\frac{C_f}{2} \frac{Re_{D0}}{Re_D}}$. The friction velocity decreases in the WT stage, except for the very early WT stage where it increases sharply from its initial value of 0.065 and attains a maximum at $Re_D = 8000$. This indicates that in the WT stage, the response of near-wall turbulence is slower than the increase in the bulk-mean velocity. u_τ/U_m increases significantly in the ST stage, where turbulence activities are enhanced with the generation of new near-wall turbulence. The shape factor decreases sharply in the early WT stage and the ST stage, followed by a gradual decrease in the PS stage. Both the displacement thickness and the momentum thickness decrease in the WT stage but increase in the ST stage (not shown here). It is interesting to note that large reductions in displacement thickness and momentum thickness have been observed also in the spatially accelerating flow (Piomelli, and Balaras, 2000).

The unsteady mean velocity profiles are shown in Figure 3. It is clearly shown in Figure 3a) that the velocity away from the wall increases linearly by the acceleration, while the velocity in the near wall region responds in a non-linear manner as shown in Figure 2b). As a result, there is an undershoot in the log-law profile in the early WT stage, and an overshoot in the late WT stage and the ST stage (Figure 3b). The velocity profiles followed the law of the wall in the PS stage as expected.

The root-mean-square velocity fluctuations are shown in Figures 4 and 5. The velocities are normalised by the initial bulk-mean velocity U_{m0} in Figure 4, and by the local friction velocity u_τ in Figure 5. One of the important features

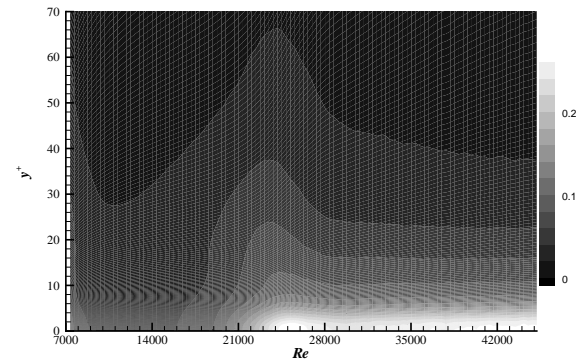
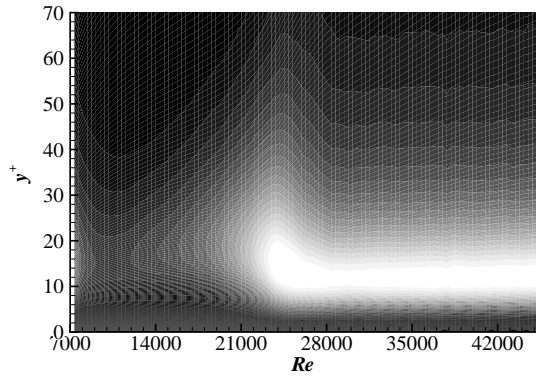
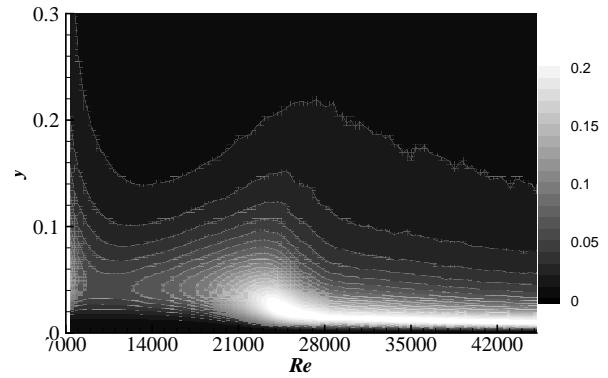


Figure 7: Turbulent kinetic energy budgets in wall units: a) production term, b) production term and c) dissipation term.

of the response of velocity fluctuations to the acceleration is a 'delay' effect (He and Jackson, 2000; Chung and Jung, 2008). It is clear from Figure 4 that the magnitudes of the all velocity fluctuations change very little during the early WT period, and the response of v and w components is even much slower. In Figure 5, it is quite clear that the response to the temporal acceleration of different velocity components is different from each other, although v and w components have somewhat similar behaviour. The axial velocity fluctuations start to increase at $Re_D = 10000$, and this rapid increase is closely associated with the turbulence production near the wall (see Figure 7a). Compared to the axial velocity fluctuations, the radial and azimuthal velocity fluctuations exhibit similar but stronger delays. v and w start to increase much later at $Re_D = 17000$, and this behaviour can

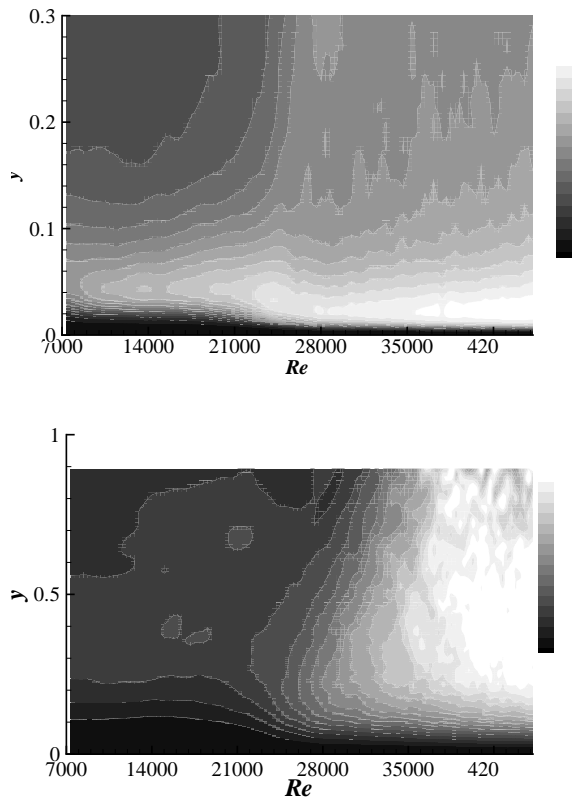


Figure 8: P/ε in wall units, and turbulent viscosity normalised by the molecular viscosity, ν_t/ν .

be attributed to the energy redistribution mechanism in the supply of energy to the v and w . In Figure 6, the behaviour of the Reynolds shear stress is similar to the lateral velocity fluctuations, and exhibits a significant delay.

Turbulence Kinetic Energy Budgets

Figure 7 shows the production term of the turbulence kinetic energy transport equation. Wall units based on the local friction velocity are used. The delay effect and the non-equilibrium state of turbulence are evident in the production term. In the early WT stage, the production term is frozen due to the slow response of the Reynolds shear stress and the mean velocity field, and the location of the peak does not change in time but remain at the initial location. So, when expressed in wall units, the peak location moves away from the wall gradually, and the magnitude of the production decreases. The production term starts to increase at $Re_D = 10000$, and this is the time when the u component begins to increase (Figure 5). As the near-wall turbulence activities become stronger in the ST stage, the location of the peak moves towards the wall, and in the PS stage, the peak is located at around $y^+ = 12$ as in the steady boundary layer. The dissipation term responds much later until in the ST stage.

The turbulent viscosity ν_t was calculated from the LES results and is shown in Figure 8. The response of ν_t to the acceleration is very slow and ν_t changes very little in the WT stage. After a long delay, it starts to increase in the ST stage, and keeps increasing until the late PS stage. At the end of the PS stage, ν_t is two orders of magnitude larger than

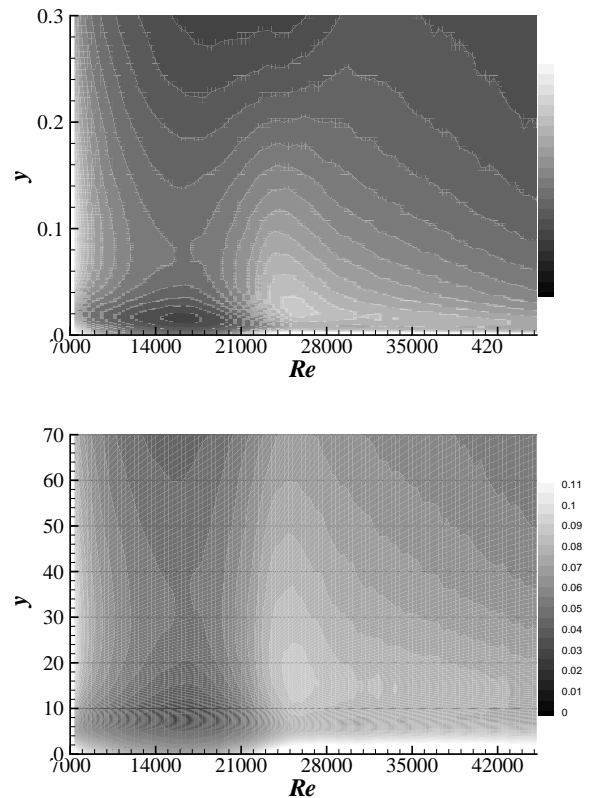


Figure 9: The streamwise vorticity fluctuations in wall units, ω_x^+ .

the laminar value. This result suggests that the enhanced anisotropy of the turbulence during the transient would be a challenging problem to standard turbulence models.

Turbulent Structures

Figure 9 shows the streamwise vorticity fluctuations in wall units. The wall normal distance is both in global units and wall units. The strength of the streamwise vorticity decreases immediately after the onset of the acceleration, and reaches a minimum at around $tU_{m0}/R = 6$ (or $Re_D = 16000$). During this period, the locations for the local minimum and maximum values remain unchanged in global units (Figure 9a), suggesting that the streamwise vortices are frozen in this stage and yet to respond to the temporal acceleration. The increase in wall shear stress (shown in Figure 2a) has not affected the near-wall turbulent structures, and the vorticity distribution does no longer bear a similarity to the equilibrium state in wall units. As shown in Figure 9b), the location for the local maximum moves gradually away from the wall in wall units, and at $tU_{m0}/R = 6$ the local maximum occurs at $y^+ = 35$. It is interesting to note that $tU_{m0}/R = 6$ is the time when the streamwise velocity fluctuations start to respond to the temporal acceleration. For $tU_{m0}/R > 6$, the streamwise vorticity fluctuations recover slowly but maintain lower values than the initial value. The local maximum value increases until $tU_{m0}/R = 13$ (or $Re_D = 25000$) in the ST stage. In the ST stages, the increase in wall shear stress starts to affect the near-wall streamwise vorticity fluctuations, and the locations for the local maximum and minimum move towards wall, and in the late ST stage, the local maximum occurs

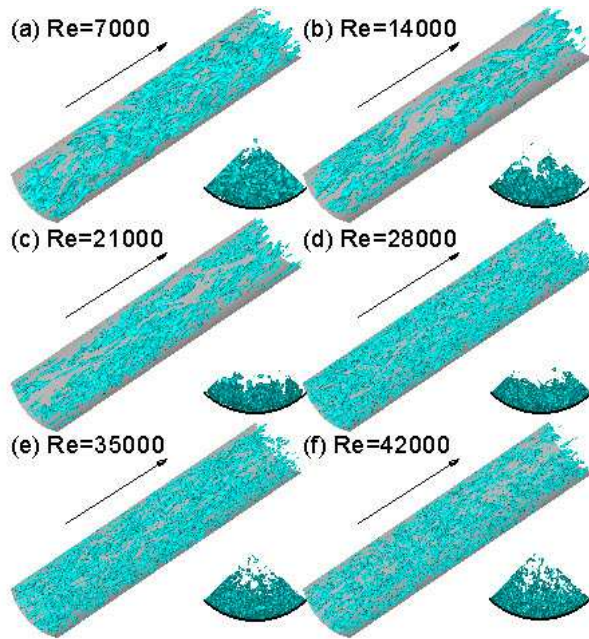


Figure 10: Instantaneous vortical structures

at $y^+ = 20$ (Kim *et al.*, 1987). For $tU_{m0}/R > 13$, the local maximum decreases and it is due to the increased dissipation at this stage, as shown in Figure 7c).

To explain the alteration of vortical structures in the transient turbulent pipe flow, we adopt the vortex identification method of Jeong and Hussain (1995). Figure 10 illustrates several snapshots of the instantaneous vortical structures. It is clear that in the WT stage, vortical structures are attenuated significantly due to the delay of turbulence production, and the flow structures at $Re_D = 14000$ are even much weaker than those at the initial Reynolds number ($Re_D = 7000$). In the ST stage ($Re_D = 21000$), the delayed turbulence production and the energy redistribution initiate the generation of new near-wall vortical structures, and at the end of ST stage, the near-wall turbulence structures were fully recovered. However, the radial propagation of turbulent structures continues in the PS stage ($Re_D > 28000$), and the flow structures in the pipe centre region does not recover fully until much later $tU_{m0}/R > 20$ ($Re_D > 35000$).

CONCLUSIONS

Large eddy simulations of unsteady turbulent pipe flow were performed to investigate the response of transient turbulence to temporal acceleration. The response of the transient flow after the onset of the acceleration was divided into three stages, based on the unsteady skin-friction behaviour: weak time-dependence (WT), strong time-dependence (ST), and pseudo-steady (PS) stages. After an initial delay, flow quantities increased rapidly in the ST stage, and recovered almost the corresponding steady value at the end of the ST stage. From the analysis of velocity fluctuations it was found that the anisotropy of the turbulence was enhanced during the acceleration due to the turbulence production and energy redistribution, and this would be a challenging problem to conventional turbulence models. The turbulent viscosity showed a long delay in the WT stage, followed by a rapid increase in the ST stage. Some similarities between the tem-

porally accelerated flow and the spatially accelerating flow have been observed.

ACKNOWLEDGEMENTS

The work is sponsored by the EPSRC (EP/D044073/1). Computer resources were provided by the Centre for Scientific Computing, University of Warwick. SYJ's visit to Warwick was supported by the Korea Research Foundation (KRF-2006-214-D00018).

REFERENCES

- Akselvoll, K., and Moin, P., 1996, "An efficient method for temporal integration of the Navier-Stokes equations in confined axisymmetric geometries", *Journal of Computational Physics*, Vol. 125, 454.
- Brodkey, R. S., Wallace, J. M., and Eckelmann, H., 1974, "Some properties of truncated turbulence signals in bounded shear flows", *Journal of Fluid Mechanics*, Vol. 63, 209.
- Chung, Y. M., 2005, "Unsteady turbulent flow with sudden pressure gradient changes", *International Journal for Numerical Methods in Fluids*, Vol. 47, 925.
- Chung, Y. M., and Jafarian, M. M., 2005, "Direct numerical simulation of unsteady decelerating", *Proceedings, 4th Turbulence and Shear Flow Phenomena*, J. A. C. Humphrey et al., ed., , Vol. 1, pp. 319–423.
- Chung, Y. M., and Jung, S. Y., 2008, "Response of near-wall turbulent flow to temporal acceleration", *Proceedings, 7th European Fluid Mechanics Conference*, J. A. C. Humphrey et al., ed., .
- Germano, M., Piomelli, U., Moin, P., and Cabot, W. H., 1991, "A dynamic subgrid-scale eddy viscosity model", *Physics of Fluids A*, Vol. 3, 1760.
- Greenblatt, D., and Moss, E. A., 2004, "Rapid temporal acceleration of a turbulent pipe flow", *Journal of Fluid Mechanics*, Vol. 514, 65.
- He, S., and Jackson, J. D., 2000, "A study of turbulence under conditions of transient flow in a pipe", *Journal of Fluid Mechanics*, Vol. 408, 1-38.
- Lilly, D. K., 1992, "A proposed modification of the Germano subgrid-scale closure method", *Physics of Fluids A*, Vol. 4, 633.
- Kataoka, K., Kawabata, T., and Miki, K., 1975, "The start-up response of pipe flow to a step change in flow rate", *Journal of Chemical Engineering Japan*, Vol. 8, 266.
- Kim, J., Moin, P., and Moser, R., 1987, "Turbulence statistics in fully developed channel flow at low Reynolds number", *Journal of Fluid Mechanics*, Vol. 177, 133.
- Kim, K., Baek, S.-J., and Sung, H. J., 2002, "An implicit velocity decoupling procedure for the incompressible Navier-Stokes equations", *International Journal for Numerical Methods in Fluids*, Vol. 38, 125.
- Maruyama, T., Kuribayashi, T., and Mizushima, T., 1976, "The structure of the turbulence in transient flows", *Journal of Chemical Engineering Japan*, Vol. 9, 431.
- Piomelli, U., Balaras, U., E., and Pascarelli, A., 2000, "Turbulent structures in accelerating boundary layers", *Journal of Turbulence*, Vol. 1, 001.
- Verzicco, R., and Orlandi, P., 1996, "A finite-difference scheme for three-dimensional incompressible flows in cylindrical coordinates", *Journal of Computational Physics*, Vol. 123, 402.
- Willmarth, W. W., and Lu, S. S., 1972, "Structure of the Reynolds stress near the wall", *Journal of Fluid Mechanics*, Vol. 55, 65.